Deformation and fracture of a directionally solidified NiAl–28Cr–6Mo eutectic alloy

X. F. Chen[a] and D. R. Johnson
Materials Science and Engineering Department, University of Tennessee, Knoxville, Tennessee 37996-2200

R. D. Noebe
NASA-Lewis Research Center, Cleveland, Ohio 44135

B. F Oliver
Materials Science and Engineering Department, University of Tennessee, Knoxville, Tennessee 37996-2200

(Received 21 June 1994; accepted 17 January 1995)

A directionally solidified alloy based on the NiAl–(Cr, Mo) eutectic was examined by transmission and scanning electron microscopy to characterize the microstructure and room temperature deformation and fracture behavior. The microstructure consisted of a lamellar morphology with a ⟨111⟩ growth direction for both the NiAl and (Cr, Mo) phases. The interphase boundary between the eutectic phases was semicoherent and composed of a well-defined dislocation network. In addition, a fine array of coherent NiAl precipitates was dispersed throughout the (Cr, Mo) phase. The eutectic morphology was stable at 1300 K with only coarsening of the NiAl precipitates occurring after heat treatment for 1.8 ks (500 h). Fracture of the aligned eutectic is characterized primarily by a crack bridging/renucleation mechanism and is controlled by the strength of the semicoherent interface between the two phases. However, contributions to the toughness of the eutectic may arise from plastic deformation of the NiAl phase and the geometry associated with the fracture process.

I. INTRODUCTION

Many ordered intermetallic alloys such as NiAl possess a unique combination of properties, making them attractive for high temperature applications. These advantageous properties include high melting point, high thermal conductivity, low density, and excellent oxidation resistance. Yet, the use of most ordered intermetallic alloys as structural components has been limited due to their brittleness at room temperature. However, improvements in the room temperature fracture toughness of NiAl-based alloys are achievable through the production of multiphase materials.[1,2]

An example of a successfully toughened system is the NiAl–34Cr eutectic[1,3] (all compositions are given in atomic percent). The NiAl–34Cr eutectic is characterized by a fibrous microstructure consisting of chromium rods embedded within a NiAl matrix.[4,5] However, molybdenum additions to the NiAl–Cr eutectic will change the microstructure from a fibrous reinforcing morphology to a lamellar morphology with a {112} type facet plane between the phases.[4] In terms of fracture resistance, a lamellar morphology is more desirable than a fibrous structure since the crack front does not have continuous access to the brittle matrix.[6] Indeed, promising room temperature fracture toughness values, much greater than that of binary NiAl, have been measured for aligned material produced by directional solidification of the lamellar NiAl–28Cr–6Mo eutectic.[1] The directionally solidified NiAl–28Cr–6Mo has an average fracture toughness of 21 MPa$\sqrt{m}$,[1] while polycrystalline NiAl has a fracture toughness of approximately 6 MPa$\sqrt{m}$.[7,8]

The improved toughness of the eutectic microstructure is provided primarily by a crack bridging/renucleation mechanism,[1,6] though crack bridging alone does not fully account for the increase in crack resistance.[1,8] Furthermore, it is somewhat surprising given the brittle nature of recrystallized chromium alloys that the room temperature toughness of the eutectic is as great as that reported. Consequently, the purpose of this paper is to characterize further the toughening mechanisms in this alloy by transmission electron microscopy (TEM) and scanning electron microscopy (SEM) techniques.

II. EXPERIMENTAL PROCEDURE

A vacuum induction melted and drop cast ingot of NiAl–28Cr–6Mo was directionally solidified in the containerless mode by the electromagnetically levitated zone process using an ultrapure H atmosphere.[1] The

[a]Visiting scholar from Materials Science Department, Shanghai Jiao Tong University, People's Republic of China.

room temperature fracture toughness was determined by performing four-point bend tests on notched samples.[1] For all the bend specimens, the notch was cut perpendicular to the growth direction, which was also perpendicular to the lamellar microstructure. Most of the bend specimens were tested in the as-processed condition. However, a number of bend specimens were heat-treated at 1300 K for 1.8 ks (500 h) and air cooled prior to testing.[1]

Microhardness measurements were made on both the as-processed and heat-treated bend specimens with a standardized Vickers indenter using a 1-kg load and a dwell time of 15 s. In all cases, the Vickers indenter was oriented parallel to the growth direction of the directionally solidified material.

Transmission electron microscopy was used to characterize the microstructure and dislocation structure of the as-processed, heat-treated, and tested eutectic. Thin slices were taken from material near the fracture surface of broken bend specimens as well as the sample ends. The thin slices were made by a slow speed diamond saw and shaped into 3 mm disks. Thinning was performed by grinding and dimple grinding, followed by twin jet electropolishing in a solution of 5% perchloric acid, 95% acetic acid at 40 V and 300 K.

Scanning electron microscopy was used to characterize the fracture behavior. The sides of the bend specimens were studied under backscattered electron conditions near the notch to characterize the microcracking adjacent to the fracture surface. In all cases, the sides of the bend specimens were polished prior to testing to facilitate these observations.

III. RESULTS

Since fracture of the notched bend specimens occurred under essentially plane strain conditions, plastic deformation of the NiAl–28Cr–6Mo eutectic was constrained to only the material very close to the fracture surface. Unfortunately, only a few TEM foils could actually be prepared from material directly adjacent to the fracture surface. Most of the TEM specimens consisted of material taken near the fracture surface but far enough away from the plastic zone to be characteristic of the as-processed material. In fact, no observable differences could be discerned between these specimens and those taken from the ends of the bend specimens. Hence, the TEM observations are divided between those from the as-processed material and those from the deformed material directly behind the fracture surface.

A. TEM observations of as-processed material

The microstructure of the NiAl–28Cr–6Mo eutectic consists of a lamellar second phase morphology as shown in Fig. 1(a). The selected area diffraction pattern of the entire area, Fig. 1(b), established a cube-on-cube crystallographic relation between the NiAl matrix and chromium phase, consistent with previous reports.[4] Diffraction patterns obtained parallel to the growth direction of the crystal also indicate a ⟨111⟩ growth direction for both phases. A semicoherent interface exists between NiAl and the refractory metal component due to the very small lattice mismatch between the two phases. An example of the network of interface dislocations that constitute a typical interphase boundary is shown in Fig. 2(a). These observations are also consistent with the earlier work of Walter *et al.* performed in the 1970's.[9,10]

While the microstructure of the as-processed eutectic was basically similar to that reported by Cline *et al.*,[4,9,10] there was one major exception. In the NiAl–28Cr–6Mo alloy, a fine array of coherent NiAl precipitates were observed in the (Cr, Mo) phase [Fig. 2(b)]. Such an array of precipitates were not observed in the fibrous NiAl–34Cr eutectic previously examined.[1]

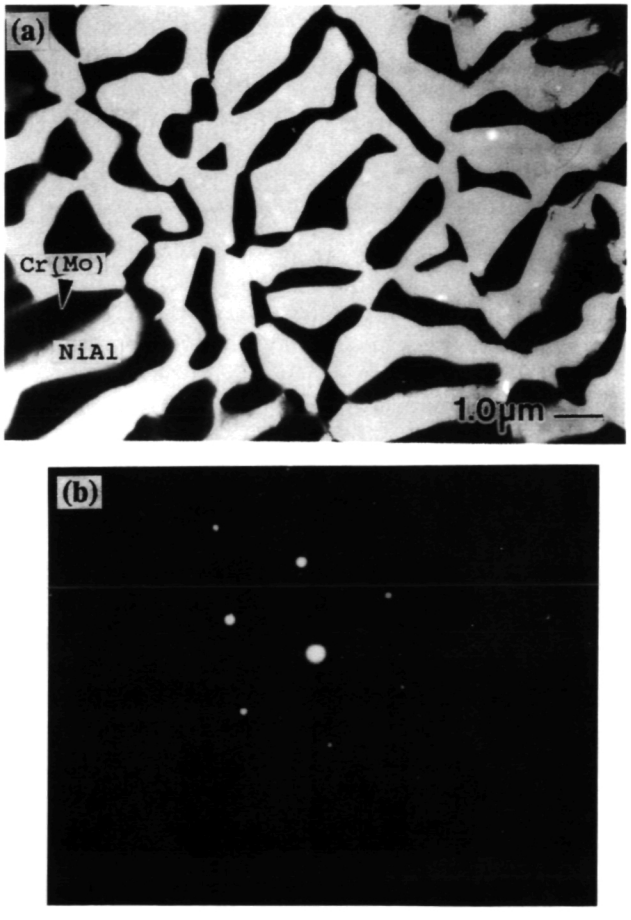

FIG. 1. TEM photomicrograph of a directionally solidified NiAl–28Cr–6Mo alloy showing (a) the lamellar morphology and (b) the corresponding diffraction pattern of ⟨111⟩ growth direction. The plane of the foil was perpendicular to the crystal growth direction.

Since the network of interface dislocations is immobile and constrained to lie along the interface, the existence of the dislocation network will strengthen the material by providing obstacles for dislocation motion. As shown in Fig. 3, the dislocations in the NiAl phase are often pinned by the interfacial dislocation network. In addition, a number of "secondary dislocations" that are not inherent to the original dislocation network were observed in all the material examined. These secondary dislocations are shown in Fig. 4 and are comparable to the extrinsic grain boundary dislocations commonly observed in polycrystalline NiAl alloys.[11,12] In both cases, lattice dislocations from the NiAl become entrapped at an interface. For polycrystalline NiAl the interface is the grain boundary between two grains, while in the eutectic alloy the dislocations become entangled at the interphase boundary. For example, Fig. 4(b) shows several lattice dislocations that are only partially absorbed into the

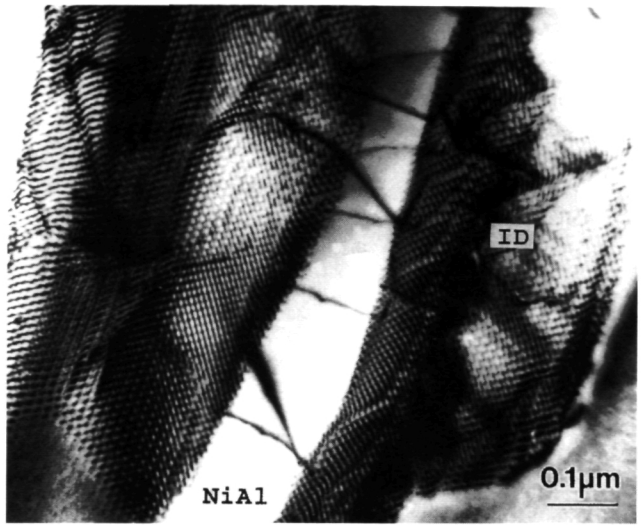

FIG. 3. TEM photomicrograph of dislocations pinned at the NiAl/(Cr, Mo) interface.

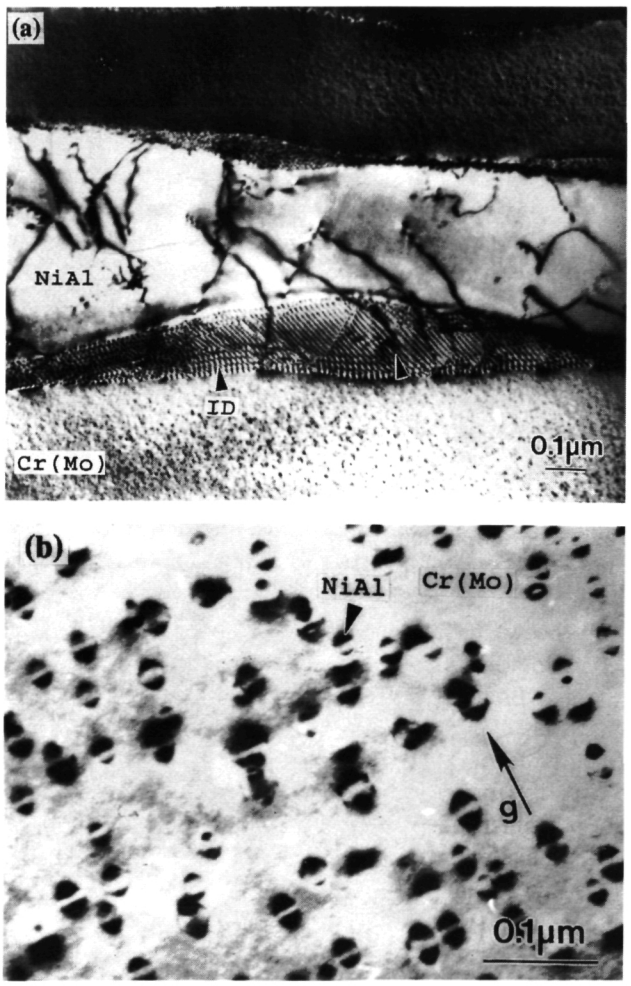

FIG. 2. A TEM photomicrograph of as-processed NiAl–28Cr–6Mo eutectic showing (a) the network of interface dislocations (ID) produced by the mismatch between the NiAl and (Cr, Mo) lattices and (b) the fine array of coherent precipitates in the (Cr, Mo) phase. Coherency is indicated by the strain contrast, $\mathbf{g} = [100]$.

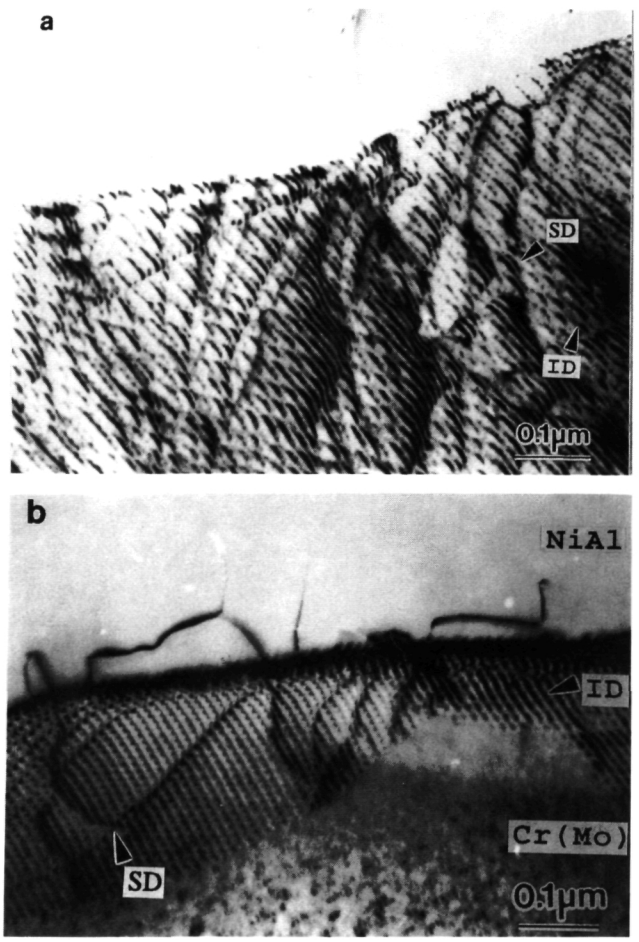

FIG. 4. TEM photomicrographs showing (a) secondary dislocations (marked SD) within the interfacial dislocation network (marked ID) and (b) a secondary dislocation extending from the NiAl and becoming absorbed by the phase boundary or interface dislocations network.

interphase boundary. Deformation of the material would cause the remaining dislocation segments to become entrapped at the boundary until the entire dislocation lines were absorbed.

B. TEM observation of deformed material

Nonuniform deformation of the lamellar eutectic characterizes the material near the fracture surface. As shown in Fig. 5, the dislocation density in NiAl is the highest along the NiAl/(Cr, Mo) interface, especially along the sections where NiAl lamellar width is small. For the particular TEM foil shown in Fig. 5, no further dislocations near the center of the NiAl lamellae (marked in the figure) could be brought into contrast by tilting the specimen.

Dislocation generation from the interface into the NiAl phase is possible, as seen in Fig. 6. Due to the fine eutectic spacing, these dislocations would be quickly pinned by neighboring interfaces. However, operation of similar sources throughout the material probably leads to the high dislocation density observed throughout the NiAl phase in both as-processed and tested samples. The Burgers vector for the dislocations in the NiAl phase was determined using the invisibility criterion $\mathbf{g} \cdot \mathbf{b} = 0$, as shown in Fig. 7 and Table I. All the dislocations were found to have a ⟨100⟩ Burgers vector consistent with previous reports of various NiAl-based materials.[13–16]

Near the fracture plane in the deformed samples, the dislocation density for the NiAl phase was much greater than that of the (Cr, Mo) solid solution (Fig. 8). In fact, very few dislocations were ever observed in the (Cr, Mo) phase. A similar result was previously found for the fibrous NiAl–34Cr eutectic.[13] For the NiAl–34Cr eutectic, the yield strength of the chromium phase was greater than that of the NiAl matrix.[1,13] For the NiAl–28Cr–6Mo eutectic, the yield strength of the refractory metal phase is further increased by both solid solution hardening due to the molybdenum addition and by precipitation hardening due to the presence of fine NiAl precipitates. Therefore, except for very localized regions, which will be discussed shortly, plastic deformation in the eutectic is concentrated in the NiAl phase during notched bend testing.

C. TEM observation after heat treatment at 1300 K

There was little change in the eutectic morphology after heat treatment at 1300 K for 1.8 ks (500 h). The microstructure of the heat-treated specimens still consisted of a fine eutectic spacing and the characteristic network of interface dislocations (Fig. 9). Consequently, the fracture toughness of the NiAl–28Cr–6Mo was similar to that of the as-processed specimens (near 21 MPa$\sqrt{\text{m}}$). There were only two notable changes in the heat-treated samples.

The first was the coarsening of precipitates found in the (Cr, Mo) phase. As shown in Fig. 10, these precipitates are disk shaped and form a semicoherent interface with the matrix as indicated by both the strain contrast and the interface dislocation network. The precipitates were determined to be NiAl. A selected area diffraction pattern and the corresponding dark-field TEM photomicrograph of the NiAl precipitates, relative to the [100] diffraction spot, are shown in Fig. 11.

The second notable change was the observation of dislocations in the (Cr, Mo) phase [Fig. 10(c)]. This observation was characteristic of the heat-treated material. Dislocations in the (Cr, Mo) phase was observable in a number of foils taken both near and away from the fracture surface. However, the dislocation density in the (Cr, Mo) phase was still very low and much less than

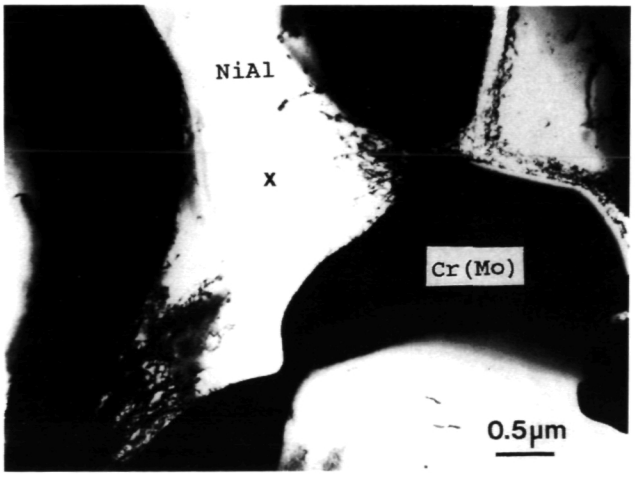

FIG. 5. TEM photomicrograph from material behind the fracture surface showing nonuniform deformation in NiAl and a very high dislocation density along the phase boundaries. No further dislocations could be brought into contrast at the center of the NiAl phase (marked with an X).

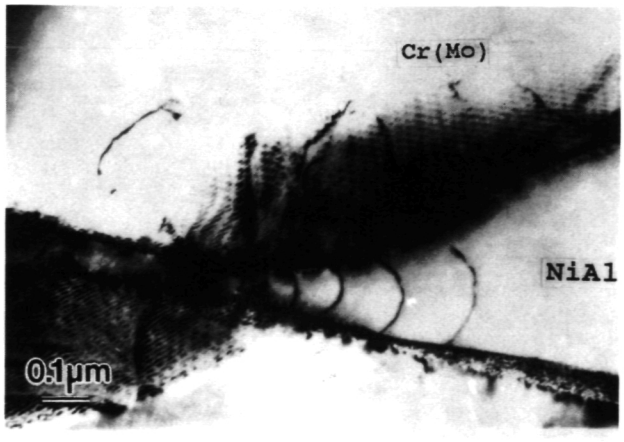

FIG. 6. TEM photomicrograph showing how the NiAl(Cr, Mo) interface may act as a dislocation source in NiAl.

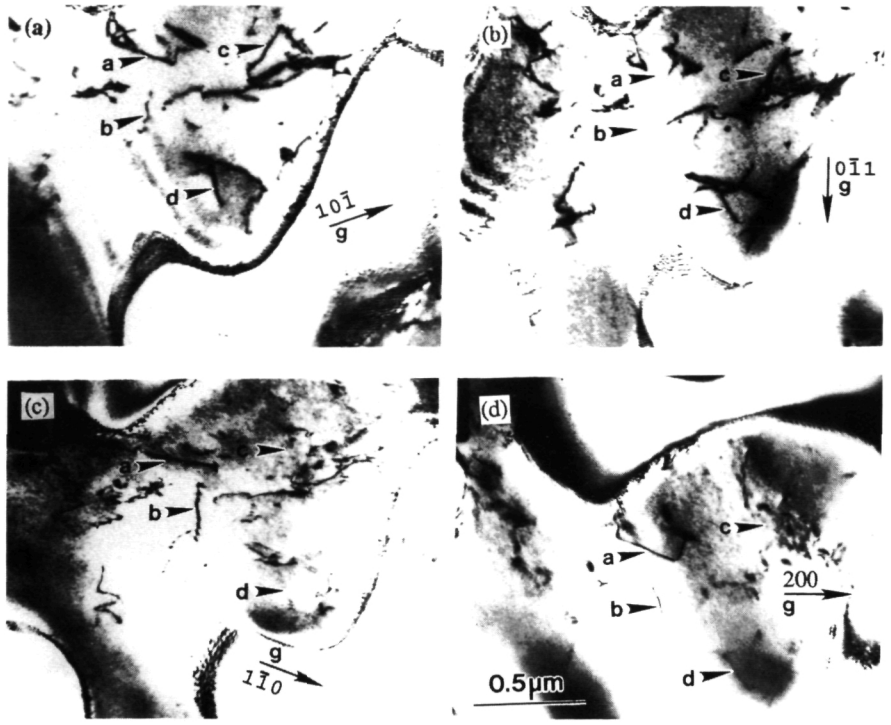

FIG. 7. TEM photomicrographs showing the determination of the ⟨100⟩ Burgers vector for dislocations in NiAl. (a) Dislocations marked a, b, c, and d are all visible for a [10$\bar{1}$] diffraction vector. (b) Dislocations marked a and b are out of contrast for a [0$\bar{1}$1] diffracting vector. (c) and (d) Dislocations marked c and d are out of contrast for a [1$\bar{1}$0] and [200] diffracting vector.

that observed in NiAl, even for foils taken very near the fracture surface.

The measured microhardness of the directionally solidified eutectic was 390 ± 5 HV for the as-processed material compared to 360 ± 5 HV for the heat-treated samples. Both the coarsening of the NiAl precipitates and the observation of dislocations in the (Cr, Mo) phase only after heat treating suggest that a decrease in the yield stress of the (Cr, Mo) phase is responsible for the lower hardness of the eutectic.

It is interesting to note that the fracture toughness of the eutectic did not change statistically with the decrease in hardness after heat treating. Therefore, similar to the as-processed and tested specimens, plastic deformation in the heat-treated material is concentrated in the NiAl phase notched bend testing. A relatively high dislocation density in NiAl for the heat-treated and tested material is shown in Fig. 12. The dislocation structure in the NiAl is characterized primarily by sharply bent dislocations, dislocation tangles, and loops.

TABLE I. Determination of the Burgers vector for dislocation observed in the NiAl phase of a directionally solidified NiAl–28Cr–6Mo eutectic.

		g · b			
Dislocation in Fig. 7	**b**	**g** = 10$\bar{1}$	0$\bar{1}$1	1$\bar{1}$0	200
a	100	1	0	1	2
b	100	1	0	1	2
c	001	−1	1	0	0
d	001	−1	1	0	0

D. SEM observations

Ducticle phase toughening can be an effective method for increasing the toughness of NiAl-based

FIG. 8. TEM photomicrograph for material taken directly behind the fracture surface of a NiAl–28Cr–6Mo bend specimen, showing a very high dislocation density in the NiAl phase.

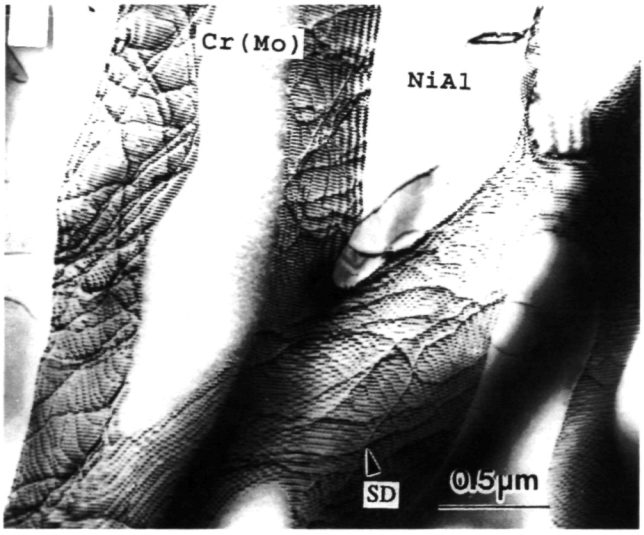

FIG. 9. TEM photomicrograph of material that had been heat-treated at 1300 K for 1.8 ks, demonstrating the stability of the eutectic microstructure and also showing the network of interface dislocations (ID) and the secondary dislocations (SD).

alloys and other intermetallic systems.[2] Typically, the increase in toughness is due to crack blunting, crack deflection, and crack bridging mechanisms. For the NiAl–28Cr–6Mo eutectic, both crack bridging and, to a much lesser extent, crack deflection mechanisms were observed (Figs. 13 and 14). However, crack blunting does not seem to contribute to the overall toughness of the eutectic. Once a crack has initiated in the NiAl phase, it will propagate until the crack front intersects the NiAl/(Cr, Mo) interface. The crack front can then be blunted by the (Cr, Mo) lamellae. However, as evidence by the low dislocation density in the (Cr, Mo) phase, NiAl deforms and fractures before any significant flow of the (Cr, Mo) takes place. Hence, the crack front is not blunted by the refractory metal phase and must either deflect along the phase boundary, cleave the chromium-rich lamella, or renucleate in the adjacent NiAl phase.

Crack bridging behavior is shown in Fig. 13. Localized necking of the refractory metal phase and partial debonding for less than 1 μm along the phase boundary are visible. Once the crack has renucleated in the adjacent NiAl lamella, the work needed to deform and fracture the bridging (Cr, Mo) phase provides a resistance to crack growth, further increasing the toughness of the composite material.

A crack deflection mechanism is shown in Fig. 14. In this photomicrograph, the crack path follows the NiAl/(Cr, Mo) phase boundary. Since the crack is redirected parallel to the principal stress direction, the stress intensity at the crack tip becomes significantly diminished, making further crack propagation difficult. However, a moderately strong bond exists at the phase

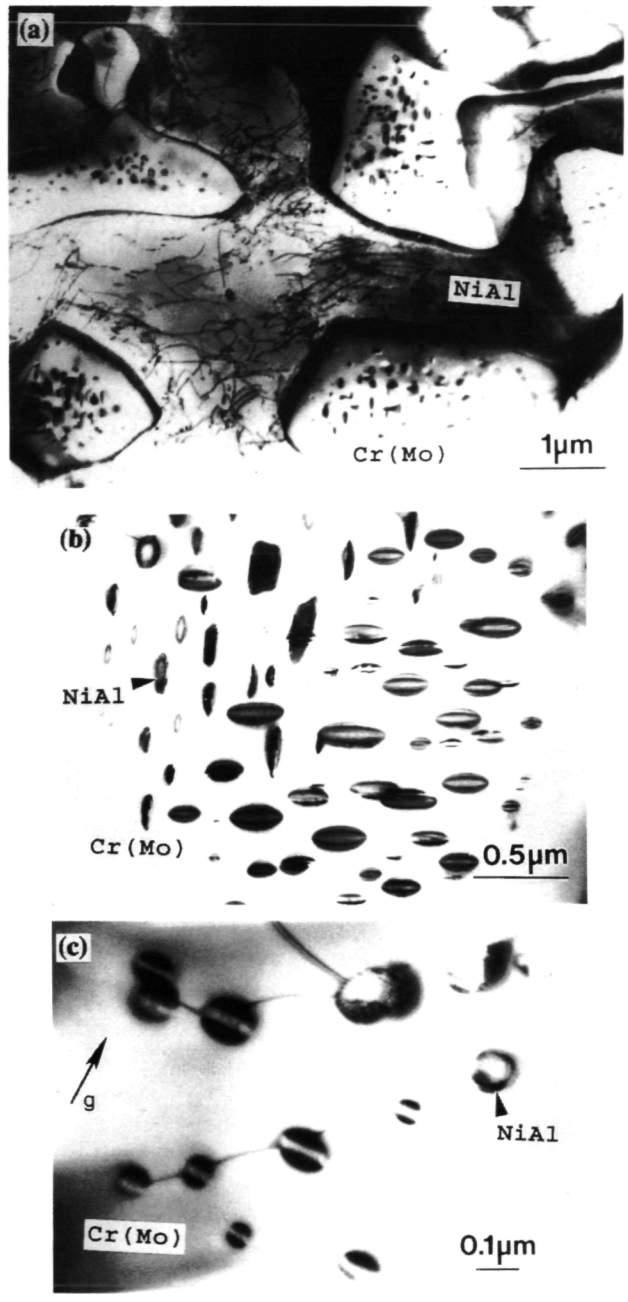

FIG. 10. TEM photomicrographs showing (a) the coarse NiAl precipitates in the (Cr, Mo) phase, (b) the disk-shaped morphology of the precipitates, and (c) the strain contrast produced by the precipitates, **g** = [100]. Dislocations are also observable in the (Cr, Mo) phase.

boundary since the two phases form a semicoherent interface. Hence, the main mode of failure is not fracture along the phase boundary, and therefore, crack deflection is not a major contributing factor to the overall toughness of the eutectic.

A typical fracture surface for the NiAl–28Cr–6Mo eutectic is shown in Fig. 15. The fracture surface is characterized by "smooth-looking" areas produced by cleavage of both the NiAl and chromium-rich lamellae

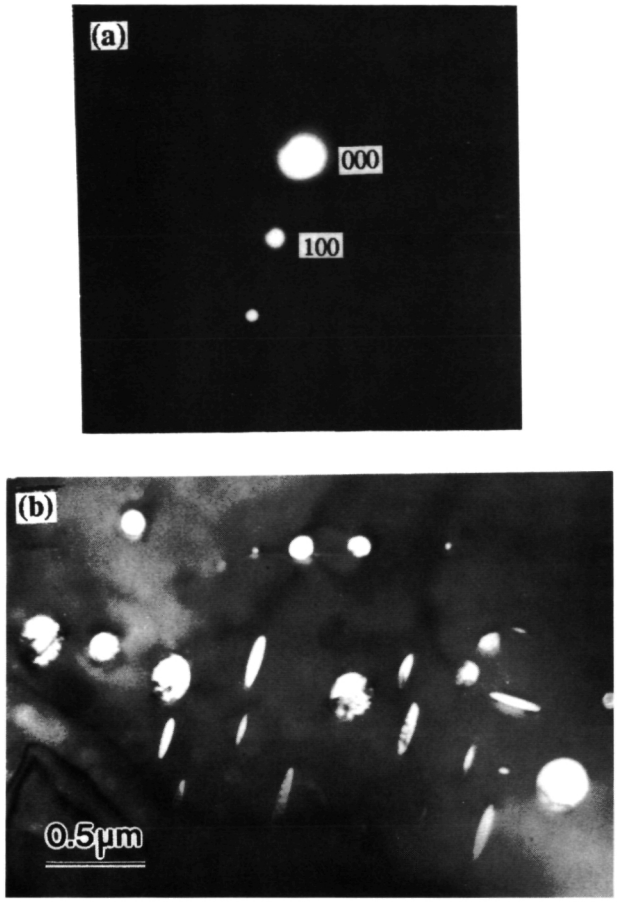

FIG. 11. TEM analysis of the NiAl precipitates in the (Cr, Mo) phase: (a) selected area diffraction pattern and (b) the corresponding dark-field image using the [100] diffraction beam, revealing the disk-shaped nature of the precipitates.

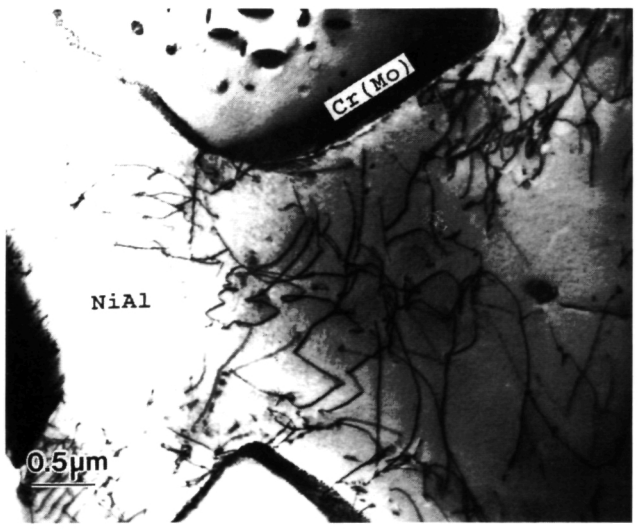

FIG. 12. TEM photomicrograph from material taken from a heat-treated and tested bend specimen showing dislocation tangles and loops in NiAl phase.

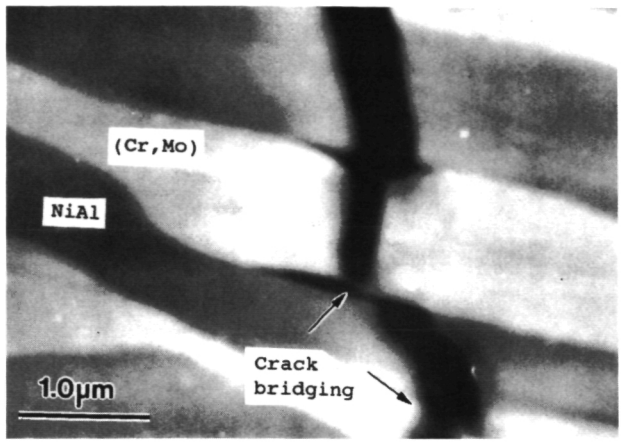

FIG. 13. SEM photomicrograph of crack bridging in a directionally solidified NiAl–28Cr–6Mo alloy.

and by "rough-looking" areas produced by a crack bridging mechanism. As shown in Fig. 15(b), the bridging chromium-rich lamella are often plastically deformed, as evidenced by their wedge-shaped fracture. In addition, the highly necked regions from the last sections of the chromium-rich lamella to fail are marked in both Figs. 13 and 15(b).

E. Fracture resistance of the constituent phases

An understanding of the fracture behavior of the individual phases that constitute the NiAl–28Cr–6Mo eutectic would be helpful in the failure analysis of the composite material. Both NiAl and chromium are typically thought of as semibrittle materials prone to cleavage fracture. The fracture toughness of the directionally solidified eutectic is much greater than that of binary NiAl.[1] However, values for the fracture toughness

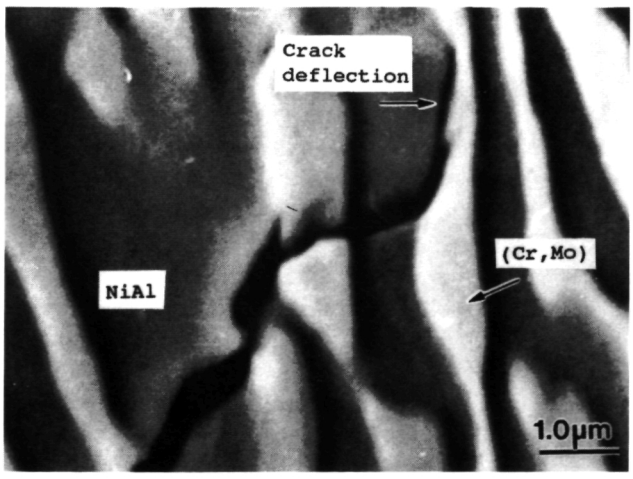

FIG. 14. SEM photomicrograph of crack deflection along the NiAl/(Cr, Mo) phase boundary.

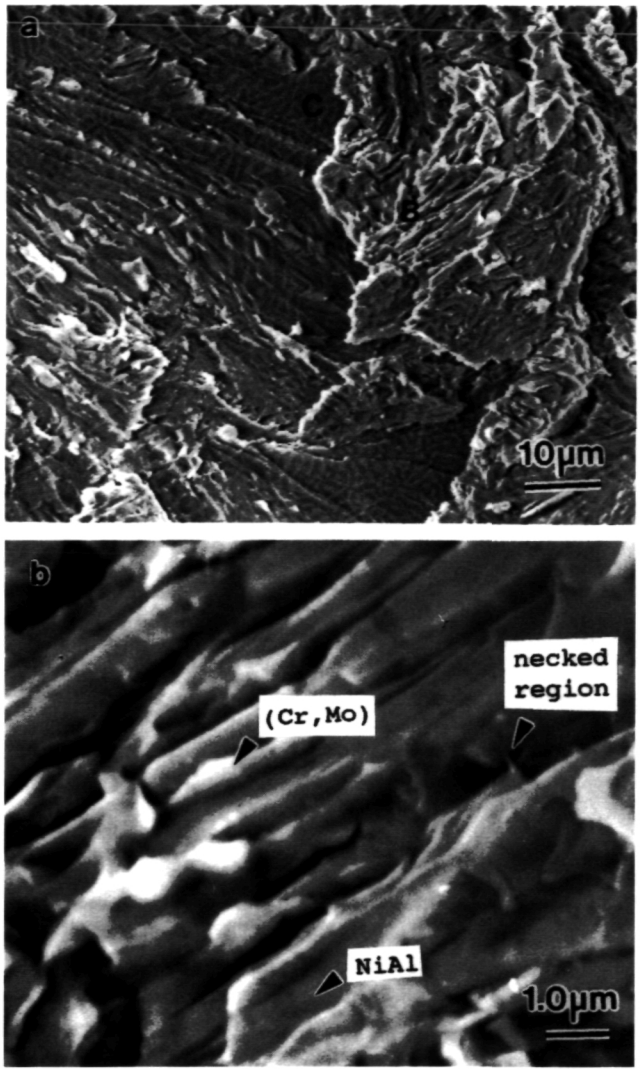

FIG. 15. SEM photomicrograph showing the fracture surface of the directionally solidified NiAl–28Cr–6Mo eutectic. (a) Cleavage fracture "smooth-looking areas" (marked by C) and crack bridging "rough-looking areas" (marked by B) are both observable on the fracture surface. (b) Fracture associated with a crack bridging mechanism. A highly necked region of a (Cr, Mo) lamellar is marked with an arrow.

of the chromium solid solution are not available. Therefore, to compare qualitatively the fracture resistance of the chromium solid solution and the NiAl–Cr-based eutectic, the fracture behavior around Rockwell-B hardness indents was examined in a series of arc-melted ingots.

Listed in Table II are the compositions and microhardness values for the arc-melted ingots.[1] Each of these ingots was polished, and five well-spaced Rockwell-B hardness indents were made in each alloy. Examination of the material around the indents indicates that chromium is significantly embrittled by additions of Ni and Al (Fig. 16). Pure chromium is quite soft, Table II, and many slip bands and no cracks were observed around the Rockwell-B indent. However, the Cr–10NiAl alloy was very brittle. No slip bands were visible at 50×, and extensive cracking was observed. Furthermore, the length of the cracks around the indents was always greater than the field of view at 50×.

In contrast, the extent of cracking around the indents for the eutectic and for the NiAl–Cr solid solution was much less. The crack length around these indents never exceeded the field of view at 50× and was typically less than the diameter of the indent. In addition, slip bands were observable at 50×, as shown in Fig. 16. Therefore, the fracture toughness of the eutectic alloy appears to be much greater than that of chromium-rich solid solution. Hence, the fracture toughness of the eutectic is greater than that of each constituent phase, and a simple of mixture analysis is not applicable.

IV. DISCUSSION

The room temperature fracture toughness of the NiAl–28Cr–6Mo is provided primarily by a crack bridging/renucleation mechanism. While the (Cr, Mo) phase did not display any generalized plasticity, there was evidence of limited plastic deformation of the chromium-rich refractory metal lamellae segments that bridged the crack path. This deformation behavior took the form of very localized wedge-shaped necks on the (Cr, Mo) lamellae. The localized plastic flow of the (Cr, Mo) phase can be explained in terms of the compressive constraint developed in the two-phase material during the fracture process. Deformation of the eutectic is nonuniform, and the stress state may become quite complex in localized regions; however, for illustrative purposes, only two simple loading conditions are considered in the following analysis: uniaxial tension and pure shear.

Initially, the material at the notch root is assumed to be loaded under uniaxial tension. However, once a crack has initiated, the fractured NiAl phase cannot support a tensile stress, and a shear stress must develop at the phase boundary between NiAl and the bridging chromium-rich phase. To see how each stress state may affect the failure mode of the (Cr ,Mo) phase, the resolved shear stress was calculated for each of the 12 different $\{110\}\langle 111\rangle$ slip vectors for the chromium-rich phase. The slip system

TABLE II. Vickers microhardness for arc-melted NiAl and Cr alloys heat-treated at 1100 K for 9000 s and furnaced cooled.[1]

Material	Vickers microhardness (kg/mm^2)
Cr (high purity)	189
Cr–10NiAl	589
NiAl–34 Cr (eutectic)	481
NiAl–10Cr	431
NiAl (high purity)	276

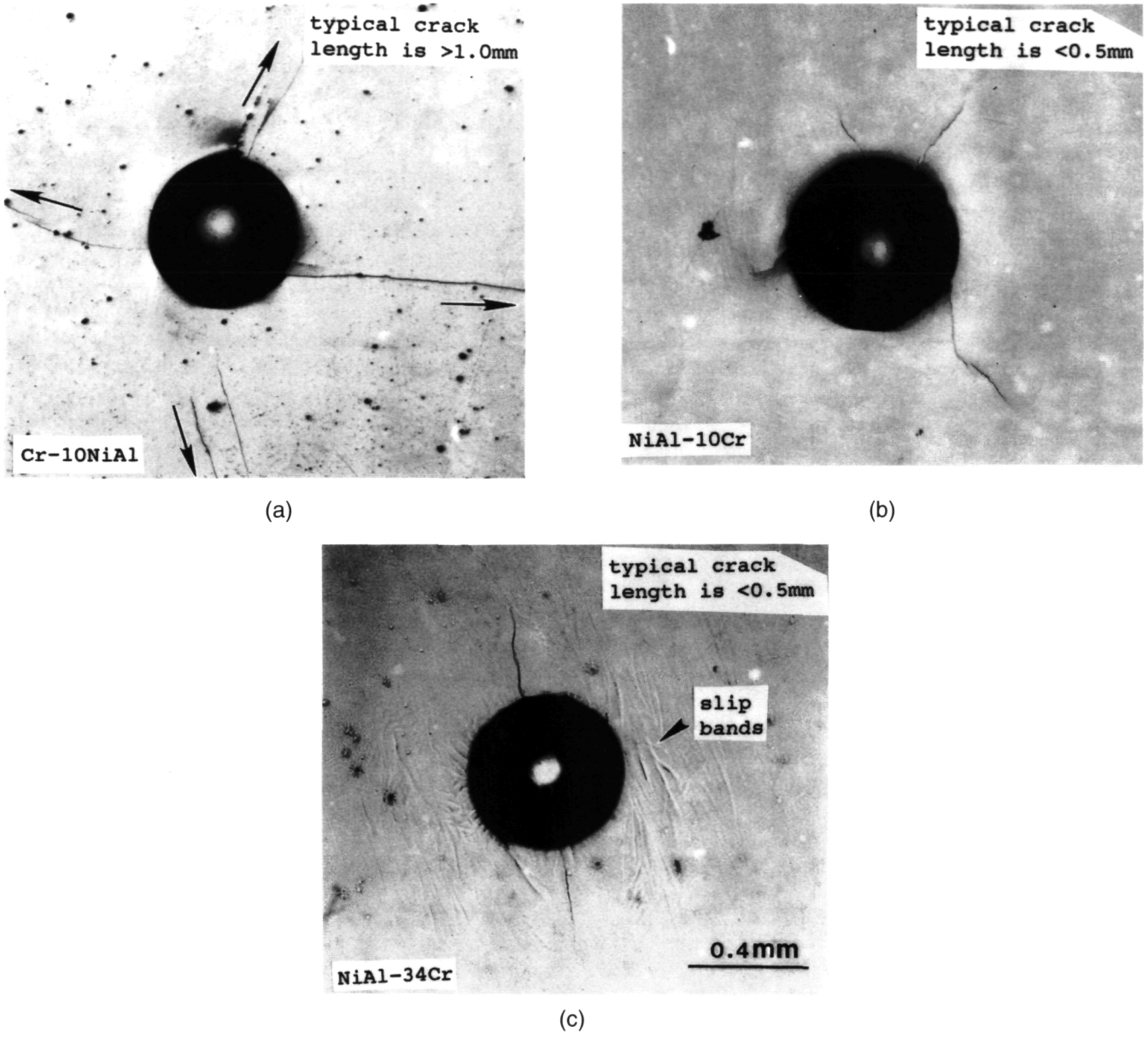

FIG. 16. Optical photomicrographs of a Rockwell-B hardness indents in arc-melted ingots. (a) Cr–10NiAl alloy showing extensive cracking around the indent. (b) NiAl–10Cr alloy with only sight cracking around the indent. (c) NiAl–34Cr eutectic showing slight cracking and slip band formation.

with the highest resolved stress was assumed to be the active system. Likewise, the normal stress produced on all the {100} cleavage planes was also calculated. These calculations were repeated over a range of orientations relative to the [111] growth direction, as illustrated in Fig. 17. The results are plotted in Fig. 18.

In Fig. 18, the resolved shear stress, τ_R, and the resolved normal stress, σ_N, on the slip and cleavage systems are normalized with respect to the magnitude of the applied stress. Why the (Cr, Mo) phase sometimes fails by cleavage instead of bridging the NiAl phase during fracture can be explained with the aid of Fig. 18(a). A very favorable orientation for cleavage (relative to the slip behavior) is found for a loading orientation rotated more than $+5°$ away from the growth direction. In contrast, for the chromium-rich lamellae oriented in the other direction ($-5°$ or more), the potential for cleavage fracture is greatly diminished and crack bridging is more likely to occur. Furthermore, should the (Cr, Mo) phase bridge the crack path, then the shear stress produced along the interface would be favorable for slip, as shown in Fig. 18(b). Both types of failure

modes for the (Cr, Mo) lamellae are observed in the same bend specimen since the eutectic microstructure can vary locally due to misalignment between adjacent eutectic cells. The local variation in microstructure of the directionally solidified NiAl–28Cr–6Mo eutectic is shown in Fig. 19.

Geometry can play another important role in the fracture resistance of the eutectic. While both phases in this case are typically thought of as semibrittle materials prone to cleavage fracture, the cleavage plane for Cr is {100}, while the cleavage plane for NiAl is {110}. Since the orientation relationship between the (Cr, Mo) lamellae and the NiAl is cube on cube, the cleavage planes will not be aligned for easy and continuous crack propagation. As a result, the crack has to change direction every time a different phase is encountered. Consequently, the crack length in the eutectic is longer than would be encountered in monolithic NiAl.

A final issue arising from this study concerns the deformation behavior of the NiAl matrix phase. In previous studies of NiAl-refractory metal eutectics, it was assumed that the NiAl phase could be modeled as an elastic medium.[1,6,8] However, observations from this study indicate that while this assumption may be appropriate as a first approximation of the behavior of the eutectic system, it is not completely valid. Evidence indicates that the NiAl phase actually undergoes significant plastic deformation in the vicinity of the crack during deformation and fracture. This is true for both the lamellar-reinforced NiAl–(Cr, Mo), Fig. 8, as well as the fiber-reinforced NiAl–Cr eutectics, Fig. 20.

The contribution to the overall toughness of the eutectic due to deformation of the NiAl phase should not be underestimated. The poor flow characteristics of binary NiAl tested in tension are in part due to the low density of mobile dislocations. Previous studies have demonstrated that a ready supply of mobile dislocations will significantly enhance the ductility,[17] fracture toughness,[18] and bend strength[19] of NiAl single crystals. For the NiAl–28Cr–6Mo eutectic, such a supply of mobile dislocations may be produced from interfacial dislocation sources that are activated by the stress field in front of the crack tip. In addition to Figs. 5 and 6, the relatively high dislocation density that is observed in NiAl prior to testing is also evidence that such interfacial dislocation sources exist. The high dislocation density in the as-processed material probably arises from interfacial dislocation sources that are activated by elastic and even plastic compatibility stresses that occur during thermal cycling due to the difference in thermal expansion coefficients of the two phases.

Lastly, the presence of the NiAl/(Cr, Mo) interface may also produce a more favorable stress state for plastic deformation of NiAl. Similar to the analysis of the (Cr, Mo) phase previously discussed, the slip and cleavage behavior of NiAl for uniaxial tension and pure shear are shown in Fig. 21. From Fig. 21(b), if a large shear stress is produced along the NiAl/(Cr, Mo) interface, then the potential for slip in NiAl is maximized while the potential for cleavage is minimized, provided that the lamellar microstructure is rotated $\pm 20°$ from the growth direction. Such a stress state may develop along the

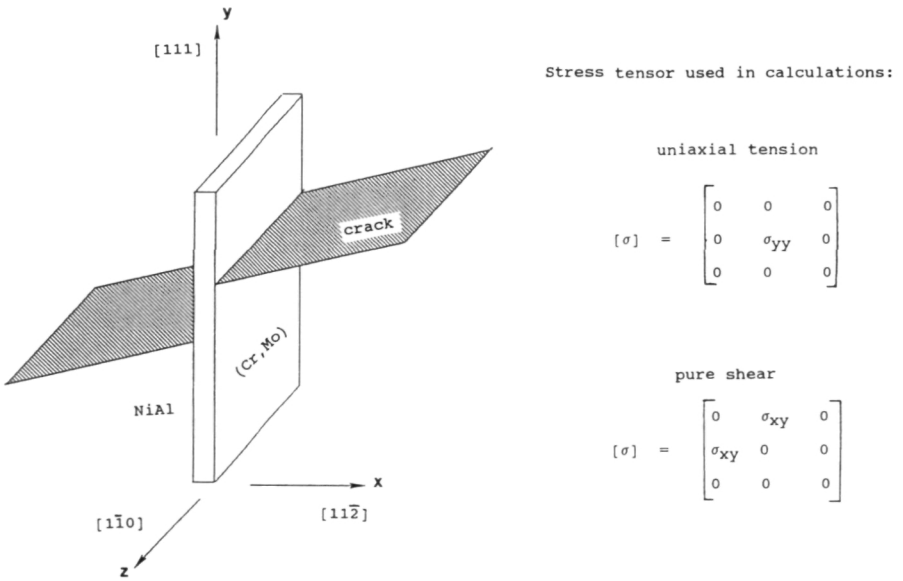

FIG. 17. Geometry of lamellar microstructure and stress tensors used in the calculations for the slip and cleavage behavior of (Cr, Mo) and NiAl.

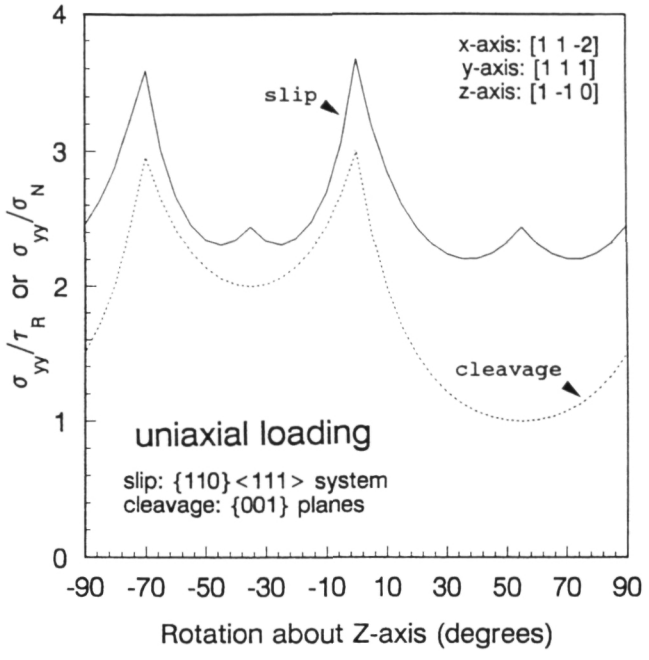

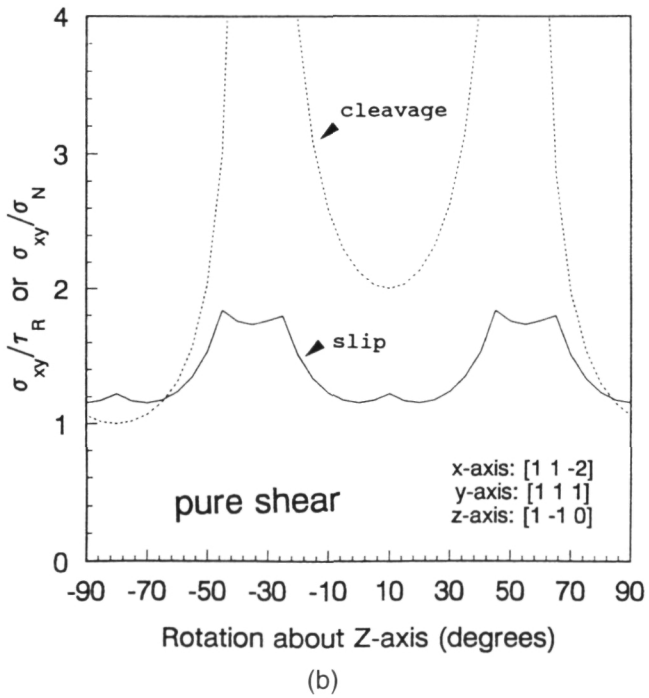

FIG. 18. Plot of how the resolved shear stress on the $\{110\}\langle 111\rangle$ slip system and how the resolved normal stress on $\{100\}$ type cleavage planes vary with loading orientation for (a) uniaxial loading conditions and (b) pure shear loading conditions for the (Cr, Mo) phase.

interface since a crack bridging mechanism is operative in the NiAl–28Cr–6Mo eutectic during fracture.

V. SUMMARY AND CONCLUSIONS

The directionally solidified NiAl–28Cr–6Mo eutectic is characterized by a lamellar microstructure with a

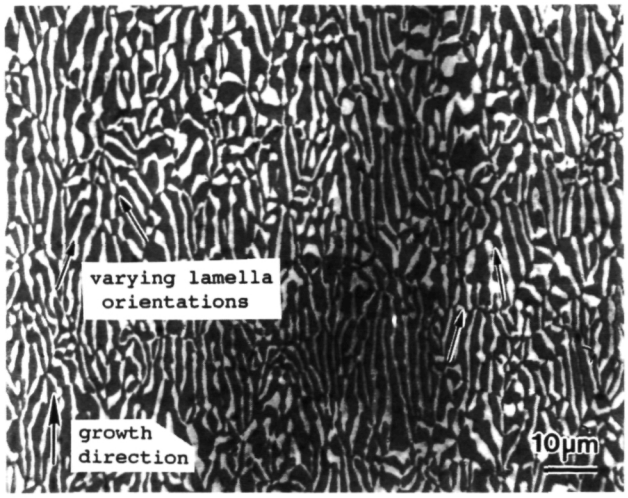

FIG. 19. Optical photomicrograph of the directionally solidified NiAl–28Cr–6Mo alloy showing the variation of the lamellar microstructure with respect to the growth direction.

$\langle 111\rangle$ growth direction for both the NiAl and (Cr, Mo) phases. The semicoherent boundary between the eutectic phases is characterized by a dislocation network at the NiAl/(Cr, Mo) interface. In addition, a fine array of coherent NiAl precipitates are dispersed throughout the (Cr, Mo) phase. The eutectic microstructure is stable at 1300 K with only coarsening of the NiAl precipitates occurring after heat treatment for 1.8 ks (500 h).

The room temperature fracture resistance of the eutectic microstructure is greater than that of the individual phases. Fracture of the aligned eutectic is characterized primarily by cleavage of both phases or by a crack bridging/renucleation mechanism. Crack deflection

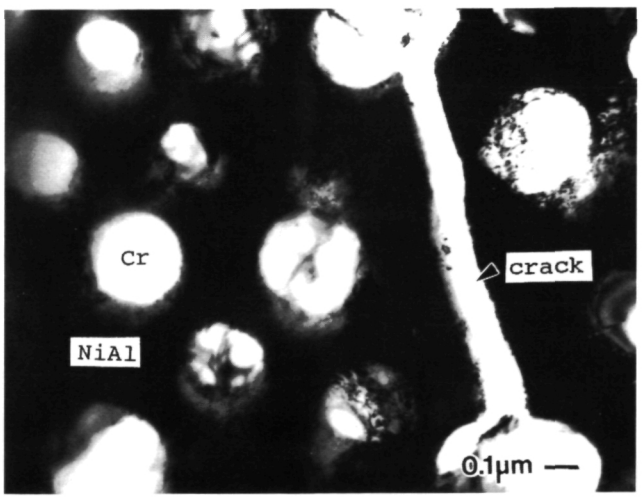

FIG. 20. TEM photomicrograph showing the extremely high dislocation density in NiAl from material in the plastic zone behind the crack front from a directionally solidified NiAl–34Cr eutectic bend specimen.

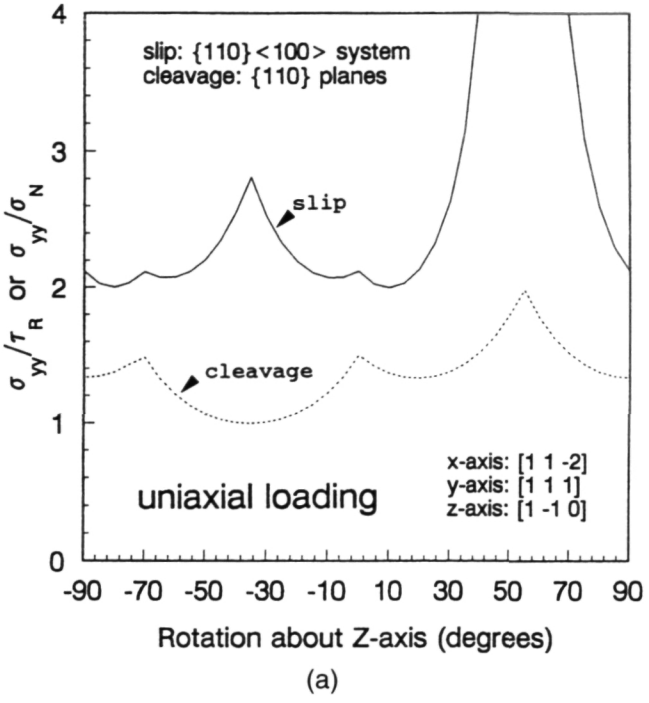

FIG. 21. Plot of how the resolved shear stress on the {100}⟨100⟩ slip system and how the resolved normal stress on {110} type cleavage planes vary with loading orientation for (a) uniaxial loading conditions and (b) pure shear loading conditions for the NiAl phase.

mechanisms may operate to a limited extent, while crack blunting is not effective in this system since the NiAl deforms and fractures before general yielding of the (Cr, Mo) phase. The good bond strength between the eutectic phases, provided by a semicoherent interface, prevents the NiAl and Cr-rich phase from acting independently. As a result of the local stress state present at the NiAl/(Cr, Mo) interface, the crack may either bridge the chromium-rich phase, deflect along the phase boundary, or simply cleave the chromium-rich lamellae. General yielding of the NiAl phase also contributes to the overall toughness of the composite material. Yielding of the phase is enhanced by an increased supply of mobile dislocations produced from interfacial sources.

ACKNOWLEDGMENTS

The authors wish to acknowledge financial and technical support from NASA Lewis Research Center through Grant NAG3-876. RDN would like to acknowledge valuable discussions with A. Misra.

REFERENCES

1. D. R. Johnson, X. F. Chen, B. F. Oliver, R. D. Noebe, and J. D. Whittenberger, Intermetallics (1994, in press).
2. R. D. Noebe, A. Misra, and R. Gibala, ISIJ Int. **31**, 1172 (1991).
3. K-M. Chang, in *Intermetallic Matrix Composites II*, edited by D. B. Miracle, D. L. Anton, and J. A. Graves (Mater. Res. Soc. Symp. Proc. **273**, Pittsburgh, PA, 1992), p. 191.
4. H. E. Cline and J. L. Walter, Metall. Trans. **1**, 2907 (1970).
5. H. E. Cline, J. L. Walter, F. Lifshin, and R. R. Russell, Metall. Trans. **2**, 189 (1971).
6. F. E. Heredia, M. Y. He, C. E. Lucas, A. G. Evans, H. E. Deve, and D. Konitzer, Acta Metall. Mater. **41**, 505 (1993).
7. K. S. Kumar, S. K. Mannan, and R. K. Viswanadham, Acta Metall. Mater. **40**, 1201 (1992).
8. F. E. Heredia and J. J. Valencia, in *Intermetallic Matrix Composites II*, edited by D. B. Miracle, D. L. Anton, and J. A. Graves (Mater. Res. Soc. Symp. Proc. **273**, Pittsburgh, PA, 1992), p. 197.
9. J. L. Walter, H. E. Cline, and E. F. Koch, Trans. AIME **245**, 2073 (1969).
10. H. E. Cline, J. L. Walter, E. F. Koch, and L. M. Osika, Acta Metall. **19**, 405 (1971).
11. R. D. Noebe, R. R. Bowman, J. T. Kim, M. Larsen, and R. Gibala, in *High Temperature Aluminides and Intermetallics*, edited by S. H. Whang, C. T. Liu, L. A. Johnson, D. P. Pope, and J. O. Steigler (The Minerals, Metals & Materials Society, Warrendale, PA, 1990), p. 271.
12. R. R. Bowman, R. D. Noebe, S. V. Raj, and I. E. Locci, Metall. Trans. **23A**, 1493 (1992).
13. X. F. Chen, D. R. Johnson, and B. F. Oliver, Scripta Metall. Mater. **30**, 975 (1994).
14. J. D. Cotton, R. D. Noebe, and M. J. Kaufman, Intermetallics **1**, 117 (1993).
15. A. Ball and R. E. Smallman, Acta Metall. **14**, 1517 (1966).
16. M. H. Loretto and R. J. Wasilewski, Philos. Mag. **23**, 1311 (1971).
17. R. D. Noebe and R. Gibala, Scripta Metall. **20**, 1635 (1986).
18. J. E. Hack, J. M. Brzeski, and R. Darolia, Scripta Metall. Mater. **27**, 1259 (1992).
19. M. A. Morris, J-F. Perez, and R. Darolia, Philos. Mag. A **69**, 507 (1994).